Review

Carbon Future

Directing photocatalysis toward practical applications from powder to films

Yifan Lin, Yuning Cai, Jiaxin Su, Guigang Zhang, Sibo Wang, Masakazu Anpo, and Yuanxing Fang

State Key Laboratory of Chemistry for NBC Hazards Protection, State Key Laboratory of Photocatalysis on Energy and Environment, College of Chemistry, Fuzhou University, Fuzhou 350108, China

Cite This: *Carbon Future* **2026**, *3*, 9200069

Read Online

ABSTRACT: Over the past three decades, substantial efforts have been dedicated to developing high-performance photocatalysts for solar fuel production and scaling up their applications, particularly through the fabrication of photocatalytic thin films. These efforts have led to significant advancements moving towards practical applications. In this review, various techniques have been introduced to achieve thin films over time, including vapor deposition, solution-phase growth, and *in-situ* polymerization, each tailored to different materials and their applications. Ultimately, the choice of method should be based on a comprehensive evaluation of factors such as efficiency, stability, process complexity, and cost in the context of solar fuel production. This review seeks to address the critical question of how to guide photoredox catalysis toward practical implementation, contributing to sustainable solutions for global energy, environmental, and other challenges.

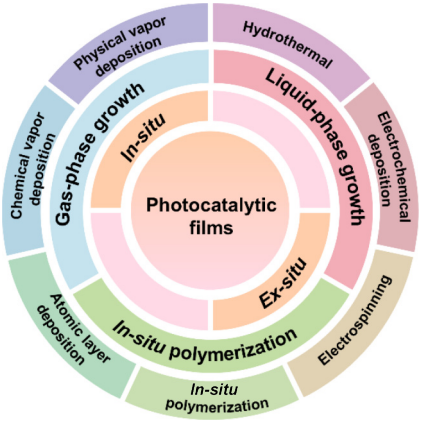

KEYWORDS: photocatalytic, films, deposition, solar to chemical conversion

1 Introduction

The escalating global energy demand and the imperative to mitigate climate change have driven intensive research into sustainable clean energy solutions. Sunlight, an abundant and inexhaustible renewable resource, delivers more energy to Earth's surface in one hour than humanity consumes annually. Despite its geographic ubiquity, solar energy remains intermittent and diffuse, necessitating efficient conversion and storage strategies[1]. Semiconductor photocatalysis, inspired by natural photosynthesis, directly transforms sunlight into high-energy-density chemical bonds via light-driven redox reactions, offering a promising avenue for sustainable solar-to-chemical energy conversion[2]. Since the discovery of photocatalysis in 1972, various semiconducting photocatalysts, including oxides, nitrides, and sulfides, have been developed[3]. A notable breakthrough was reported by Takata et al., who achieved nearly 100% quantum efficiency for overall water splitting using $SrTiO_3$:Al, significantly advancing the development of particulate semiconductor photocatalysts for practical solar hydrogen production[4]. In parallel, the discovery of polymeric carbon nitride (PCN) in 2009 had generated significant interest in metal-free semiconductors[5], due to their tunable physicochemical properties and potential for a wide range of photocatalytic applications[6–12].

However, as we move toward large-scale industrialization, a key challenge arises: How can high-performance powder catalysts be transformed into stable and easily manageable industrial systems? The inherent powder form of these catalysts presents several obstacles to this transformation. One promising solution is immobilizing the catalysts into thin films, which offers several advantages. Firstly, it eliminates the complex issue of post-reaction catalyst separation, preventing activity loss and minimizing secondary pollution. Secondly, the structured morphology of thin films overcomes the severe light scattering and shielding that typically occur with randomly agglomerated powders, ensuring better light-harvesting efficiency. Lastly, thin films are more compatible with continuous flow reactors, which improve reaction kinetics, a significant limitation in the batch reactors commonly used with powder systems[13–15]. Additionally, for economically viable solar hydrogen production through photocatalytic water splitting, it is estimated that photocatalysts must achieve a solar-to-hydrogen (STH) efficiency of over 5% and maintain a lifespan of at least 10 years[16]. To address these challenges, the design of immobilized photocatalytic films, particularly those fabricated through *in-situ* growth strategies, has regarded as a potential

Received: December 30, 2025; **Revised:** January 29, 2026
Accepted: February 27, 2026

Address correspondence to Yuanxing Fang, yxfang@fzu.edu.cn

https://doi.org/10.26599/CF.2026.9200069

approach. In practical toward expanding the light-accepting area. Therefore, developing the appropriate methods to achieve PCN films is considered a potential pathway for advancing photocatalysis toward practical applications.

This review article discusses the synthesis strategies for photocatalytic thin films used in both half and overall water splitting reactions, with a focus on *ex-situ* and *in-situ* approaches. The methods discussed include powder-based physical coating, physical vapor deposition (PVD), chemical vapor deposition (CVD), atomic layer deposition (ALD), hydrothermal/solvothermal synthesis, electrochemical deposition, electrospinning, and *in-situ* polymerization technology. For each technique, the fundamental principles, advantages, limitations, and application potential are outlined and critically evaluated in the context of large-scale solar fuel production. Additionally, this review addresses the key challenge of steering photoredox catalysis toward practical implementation, offering insights into its role in advancing sustainable solutions to global energy and environmental issues.

2 Achieve photocatalytic films and applications

2.1 Coating photocatalyst powder

Physical coating is a conventional approach for fabricating photocatalytic devices. A representative example involved the synthesis of TiO_2 films with thicknesses ranging from 20 to 100 nm via spray-coating techniques[17]. This method offers a practical route for immobilizing high-performance powdered photocatalysts in large-scale reactions. Among physical coating techniques, the casting method is widely employed, relying primarily on the physicochemical properties of the slurry, such as gravity, surface tension, capillary action, and fluidity, to spread across and fill a confined mold or substrate area. This principle necessitates slurries with low viscosity and good flowability.

A notable advantage of the casting method is its flexibility in substrate selection: It can be applied to both rigid substrates and peelable surfaces, enabling the fabrication of free-standing and self-supporting films. However, the resulting thickness of films is highly dependent on the volume and viscosity of the slurry, as well as the drying conditions. These factors contribute to significant batch-to-batch variations and poor reproducibility. Additionally, because the process relies on the natural flow of the slurry and slow solvent evaporation, it is inherently time-consuming and requires a perfectly level and vibration-free surface. These limitations pose significant challenges for scaling up the casting method to continuous industrial production.

The coating method employs external mechanical forces, such as shear force in trowel coating or centrifugal force in spin coating, to spread and deposit the slurry onto the substrate, resulting in the formation of thin and uniform films. Although this method typically requires a rigid and planar substrate, which limits substrate flexibility, it offers excellent control over uniformity of the films. By precisely tuning process parameters, such as the rotational speed in spin coating to modulate centrifugal force, the thickness and consistency of the resulting films can be effectively controlled. This high degree of control makes the coating method well-suited for large-scale synthesis and practical applications.

Typically, the photocatalytic powder was mixed with water, ethanol, or N,N-dimethylformamide (DMF), then the solution was loaded on glass substrates via drop-casting. This approach was applicable for photocatalystss, including PtSA-two dimensional metal-organic framework (2D MOF) nanosheets films[18], $Pt_{0.3}$-ZnInS thin films[19], r-covalent triazine framework (CTF) nanosheet films[20], and Cu_CNi_1/TiO_2[21]. As a notable example, Wang et al. employed a blade-coating technique in which the photocatalyst was mixed with poly vinylidene fluoride (PVDF) in 1-methyl-2-pyrrolidinone to form a uniform slurry. This slurry was then evenly applied onto aluminum foil using a glass rod, resulting in amorphous ZnCdS (AZCS)/Co-MoS_x films with an area of 400 cm^2 [22]. The observation of visible H_2 bubbled from the AZCS/Co-MoS_x films in the presence of lactic acid under both Xe lamp and natural sunlight clearly demonstrated their potential for scalable solar-driven H_2 production.

Valencia-Valero et al. fabricated a Pt/TiO_2-based flat-panel reactor via a drop-casting method, achieving a photoactive area of 1400 cm^2 (**Fig. 1a**)[23]. This reactor was employed for hydrogen production through the oxidation of urban wastewater. Under simulated sunlight irradiation, its hydrogen evolution rate is approximately 54 $\mu mol \cdot g^{-1} \cdot h^{-1}$. Over 27 days of continuous exposure to sunlight, the system consistently generated hydrogen, with the production rate fluctuating in response to solar irradiation intensity. Simultaneously, the concentration of organic pollutants in the wastewater steadily decreased. These findings demonstrated that this system represents a significant advancement in urban wastewater treatment, enabling not only the effective degradation of organic contaminants but also the sustainable production of green hydrogen.

Overall water splitting by photoredox catalysis through photocatalytic panel is known as one of the possible approaches for practical applications. Domen's group proposed distinct perspectives on the preparation of photocatalytic thin films materials applicable to this process. Gu et al. employed a straightforward filtration technique to fabricate the photocatalyst sheet (Fig. 1b)[24]. In this process, they dispersed the photocatalyst in water and filtered the mixture to remove the solvent, after which the filter paper with the retained catalyst was dried to form the final sheet. $Sm_2Ti_2O_5S_2$ (STOS) was prepared by a flux-assisted approach and modified with Cr_2O_3, Pt, and IrO_2 co-catalysts to form Cr_2O_3/Pt/IrO_2/STOS; meanwhile, $BiVO_4$ (BVO) was synthesized hydrothermally and loaded with CoO_x to obtain CoO_x/BVO. Using above method, they successfully fabricated Cr_2O_3/Pt/IrO_2/STOS-CNT-CoO_x/BVO sheets, achieving photocatalytic overall water splitting and exhibiting an STH efficiency of 0.40% under 10 kPa at 323 K.

In a different approach, Wang et al. employed a particle transfer method that involved dispersing $SrTiO_3$:La,Rh and $BiVO_4$:Mo powders in isopropanol[1]. The suspension was drop-cast onto a glass substrate, and a thin gold layer was deposited via thermal vacuum evaporation. The sample was then placed on an alumina plate and heated to 573 K to ensure good contact between the Au films and the photocatalyst particles. Afterward, the Au films with the adhered photocatalyst was bonded to a second glass plate using adhesive tape and peeled off from the original substrate, resulting in a free-standing photocatalyst sheet (Fig. 1c). The monolithic device achieves a solar-to-formate conversion efficiency of 0.08% ± 0.01% and a formate selectivity of 97% ± 3%.

Additionally, Wang et al. developed a method for preparing photocatalyst sheets using screen printing technology[25]. The printing ink was formulated by mixing catalyst powder, a Au

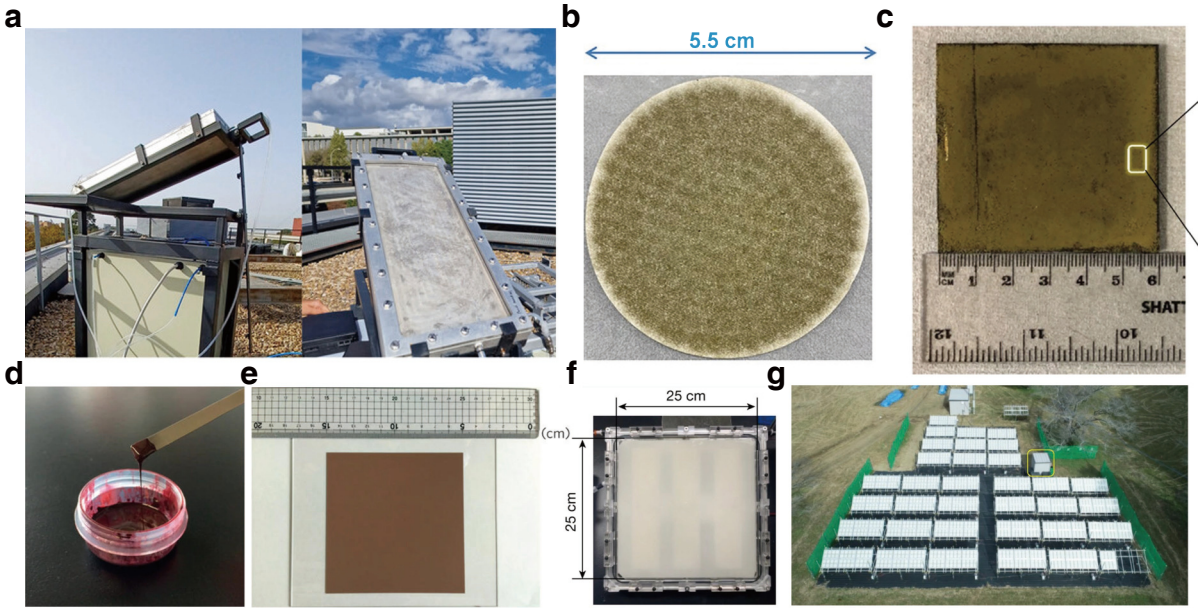

Fig. 1. **a**, Photo of a Pt/TiO_2-based flat-panel reactor with a photoactive area of 1400 cm^2. Reproduced with permission from Ref.[23], © Valencia-Valero, L. C. et al. 2025. **b**, Overhead photographic images of Cr_2O_3/Pt/IrO_2-loaded STOS and CoO_x-loaded BVO on filter paper. Reproduced with permission from Ref.[24], © Elsevier Inc. 2024. **c**, A photograph of a 6 cm × 5.7 cm CotpyP-loaded $SrTiO_3$:La,Rh|Au|RuO_2-$BiVO_4$:Mo photocatalyst sheet prepared by the particle transfer method. Reproduced with permission from Ref.[1], © Wang, Q. et al. 2020. **d**, Photograph of the ink used for screen printing the photocatalyst sheet. **e**, Photograph of a 10 cm × 10 cm $SrTiO_3$:La,Rh/Au nanoparticle/$BiVO_4$:Mo printed sheet. Reproduced with permission from Ref.[25] © Springer Nature Limited 2016. **f**, Image of the $SrTiO_3$-based panel reactor unit (625 cm^2). Reproduced with permission from Ref.[26], © Nishiyama, H. et al. 2021. **g**, An overhead view of the 100 m^2 solar hydrogen production system consisting of 1600 panel reactor units and a hut housing a gas separation facility (indicated by the yellow box). Reproduced with permission from Ref.[26], © Nishiyama, H. et al. 2021.

colloidal solution, and an organic vehicle consisting of α-terpineol, 2-(2-butoxyethoxy)ethanol, and acrylic resin in specific proportions (Figs. 1d and 1e). After evaporating the ethanol from the ink, the resulting paste was screen-printed onto a glass substrate, followed by drying and calcination to produce the corresponding photocatalyst sheets. The STH of the Ru-loaded printed $SrTiO_3$:La,Rh/Au colloid (40 wt.%)/$BiVO_4$:Mo sheet reached 0.1%, based on the average gas evolution rate over the 13-h reaction.

In 2021, Domen and co-workers reported the construction of a photocatalytic overall water splitting panel reactor array with an area of up to 100 m^2 (Figs. 1f and 1g)[26]. They systematically optimized the formation technique of films and ultimately employed a spray valve system controlled by a customized programmable *X*–*Y* robot to fabricate the photocatalyst sheets. A suspension was prepared by dispersing modified $SrTiO_3$:Al, chain-like colloidal silica, and calcium chloride in pure water at specific ratios. This mixture was then spray-coated onto frosted glass plates using the robotic sprayer, with the coating process repeated 20 times to ensure uniformity and adequate thickness. The coated sheets were subsequently dried at 90 °C under 50% relative humidity for 4 h, producing photocatalyst panels suitable for large-scale solar-driven water splitting. The resulting panel reactor array demonstrated stable and efficient operation over several months, maintaining a STH conversion efficiency of 0.76%. This achievement highlighted the practical feasibility of scaling up photocatalytic water splitting with integrated gas collection and separation systems.

In summary, although the powder coating and casting techniques have facilitated the preparation and investigation of photocatalytic films due to their operational simplicity, they suffer from a critical limitation: weak interfacial bonding. These methods typically rely on van der Waals interactions or minimal physical anchoring, which results in poor mechanical stability of the films. Under fluid flow or prolonged operation, catalyst particles tend to detach, leading to not only a decline in photocatalytic activity but also the risk of secondary contamination.

2.2 Physical vapor deposition

PVD encompasses a group of techniques carried out in a vacuum environment, where solid source materials are vaporized through physical processes, such as thermal evaporation or particle bombardment, and then condensed onto a substrate to form a thin films. Among various PVD methods, magnetron sputtering is not only the most extensively employed for fabricating photocatalytic thin films but also one of the earliest, with applications dating back to 1995 [27]. The fundamental principle involves placing the target material as the cathode and the substrate as the anode inside a vacuum chamber. A high-voltage electric field is applied to ionize the working Ar gas, generating a plasma. The resulting Ar^+ ions are accelerated toward the target, causing high-energy bombardment that ejects atoms from its surface. These atoms then deposit onto the substrate, forming thin films. Additionally, introducing reactive gases such as O_2 or N_2 allows for the direct deposition of oxide or nitride films during the process.

In 2021, Bonomi et al. reported the vapor-phase deposition of Bi-based perovskite thin films via radio-frequency (RF) magnetron sputtering[28]. The sputtering target was fabricated by pressing a stoichiometric mixture of precursors, CsBr, CsI, BiI_3, and $BiBr_3$, into a solid powder form. Using Ar as the working gas and an RF power of 50 W, $Cs_3Bi_2(Cl_{1-x}I_x)_9$ thin films were deposited onto glass substrates with an area of 6.25 cm^2. By precisely controlling the stoichiometry of the precursors, the band gap of the resulting films

was tunable, ranging from 2.0 eV for $Cs_3Bi_2I_9$ to approximately 2.64 eV for $Cs_3Bi_2Br_9$. These films demonstrated promising photocatalytic activity in the photodegradation of methylene blue.

Separately, $BiVO_4$ has been widely studied in photocatalysis due to its visible-light responsiveness and tunable morphology. Hui et al. successfully deposited amorphous $BiVO_4$ films onto mica substrates using magnetron sputtering at room temperature, employing a sputtering power of 100 W and an Ar/O_2 partial pressure ratio of 1:0.5 [29]. Post-deposition annealing in air transformed the amorphous films into a crystalline and flexible $BiVO_4$ films. Remarkably, the photocurrent of the device remained stable under different bending radii, and the films withstood over 500 bending cycles without significant degradation, demonstrating its excellent mechanical durability.

Although magnetron sputtering offers several advantages, such as low-temperature deposition, broad substrate compatibility, high films quality, versatility in material selection, reactive sputtering capability, and precise process control, it also comes with notable limitations. These include the need for high-vacuum systems, high-voltage power supplies, sophisticated gas delivery infrastructure, and strict parameter control, all of which contribute to significant initial investment and maintenance costs.

Vacuum evaporation is a technique used to produce thin films. This process is carried out under vacuum conditions, in which the coating material is vaporized through a specific heating method. The vaporized particles then travel through the vacuum and condense on the substrate surface to form a thin films. Timoumi et al. utilized this method to evaporate Cu_2AlSnS_4 powder at 300 °C. The resulting films, with a thickness of 500–600 nm, exhibited excellent photocatalytic activity for the degradation of methylene blue[30]. In addition, Ichihashi et al. deposited 5,8-dicyanopicene films onto a quartz substrate at a rate of 0.2 $nm \cdot s^{-1}$ by evaporating 5,8-dicyanopicene. They applied the films to photocatalytic water splitting for hydrogen production[31]. Under irradiation with light of $\lambda \geq 390$ nm from a 500 W xenon lamp and in the presence of formic acid, it exhibited a hydrogen evolution rate of 45.6 $\mu mol \cdot m^{-2} \cdot h^{-1}$ and maintained stability over three cycles. Despite the advantages from this technique, such as its simple principle and ease of operation, vacuum evaporation faces challenges, including poor films adhesion, limited precision in thickness control, and a tendency for fractionation during the deposition of alloys or compounds.

Molecular beam epitaxy (MBE) is a technique used to grow thin films in an ultra-high vacuum environment. In this process, thermal atomic or molecular beams of constituent elements are directed onto a heated single-crystal substrate, enabling epitaxial growth of single-crystal films in an atom-by-atom layer manner. Kraut et al. utilized an MBE system equipped with standard effusion cells for Zn and Ga, along with a radio-frequency plasma source[32]. High-purity N_2 and O_2 were mixed using mass flow controllers, allowing precise control over their ratio before being injected into the plasma source. Under a vacuum of ca. 10^{10} mbar and at a temperature of 150 °C, $(GaN)_{1-x}(ZnO)_x$ films were grown on double-side polished and single-crystalline (0001) sapphire substrates. By adjusting the flux ratios of Ga/Zn and N/O, the bandgap of $(GaN)_{1-x}(ZnO)_x$ could be tuned over a wide range from 2.0 ± 0.1 to 3.8 ± 0.2 eV, with the potential to extend up to 4.3 eV or higher. This flexibility overcame the composition limitations typically associated with GaN:ZnO solid solutions, paving the way for the development of new compounds within this material class. Although MBE allows the growth of atomic-level control over thin films, resulting in exceptionally high purity and quality, its practical application in industrial production is hindered by the extremely high equipment costs, system complexity, and very slow growth rates.

2.3 Chemical vapor deposition and atomic layer deposition

CVD is a technique used to produce solid thin films through controlled chemical reactions of gaseous or vapor-phase precursors on a substrate surface[33]. The development of CVD marks a significant evolution in growth technology of vapor-phase thin-films, transitioning from the physical "relocation" of materials in PVD to controlled chemical reactions occurring directly on the substrate surface. This shift in principle allows CVD to produce photocatalytic thin films with improved crystalline quality and more complex compositions.

CVD uses gaseous precursors with excellent diffusivity, enabling non-line-of-sight deposition. This advantage allows CVD to achieve uniform and conformal thin-films growth on substrates with complex three-dimensional structures, such as carbon cloth or porous materials. In contrast, although traditional PVD performs well on flat and rigid substrates like glass, it often struggles with uneven coverage on high-aspect-ratio or irregular surfaces. Although advanced process designs have enabled PVD to be applied to certain flexible polymer substrates, achieving uniform coverage on complex and irregular structures with PVD is generally much more challenging and costly than with CVD. For example, using CVD with SiO_2/Si particles and carbon as sources in Ar at 1500 °C, Liu et al. uniformly grew SiC nanowires on a 2 cm × 4 cm carbon fiber cloth[34].

Furthermore, because CVD involves chemical bonding rather than the high temperatures or energetic bombardment typical of PVD, CVD films generally achieve good crystallinity either during deposition or after low-temperature annealing. For photocatalytic materials, higher crystallinity typically corresponds to fewer bulk defects. In photocatalytic reactions, these defects often act as recombination centers that trap photogenerated charge carriers and facilitate their recombination, thereby reducing photocatalytic efficiency[35]. Therefore, maintaining high crystallinity is crucial for optimizing photocatalytic performance. Using a one-step chemical vapor deposition method, Lian et al. deposited Mo_2C/MoO_x films on a 2 cm × 2 cm carbon cloth[36]. The high crystallinity of the films was achieved, as shown in high resolution transmission electron microscopy (HRTEM) images and X-ray diffraction (XRD) pattern (**Figs. 2a** and 2b).

CVD is applicable to a wide range of materials, converting them into thin films. Recently, CVD has been used to fabricate metal-free photocatalysts into thin films, as the precise control over precursor flow rates enables uniform and controllable structural modulation[37]. A typical example is the application of CVD for the fabrication of carbon nitride (CN) nanorod arrays on glass slides[38]. In this approach, a melamine-cyanuric acid supramolecular precursor was placed at the bottom of a beaker, covered with a glass slide, and sealed with aluminum foil, followed by heating at 600 °C for 4 h. This method allowed the nitrogen vacancy density to be tailored by controlling the temperature, which in turn tuned the photophysical properties of the CN nanorods. The resulting CN nanorod films was then employed as a photocatalyst panel for continuous-flow photocatalytic H_2O_2 production, achieving a hydrogen peroxide yield of 14.2 $mmol \cdot m^{-2} \cdot h^{-1}$.

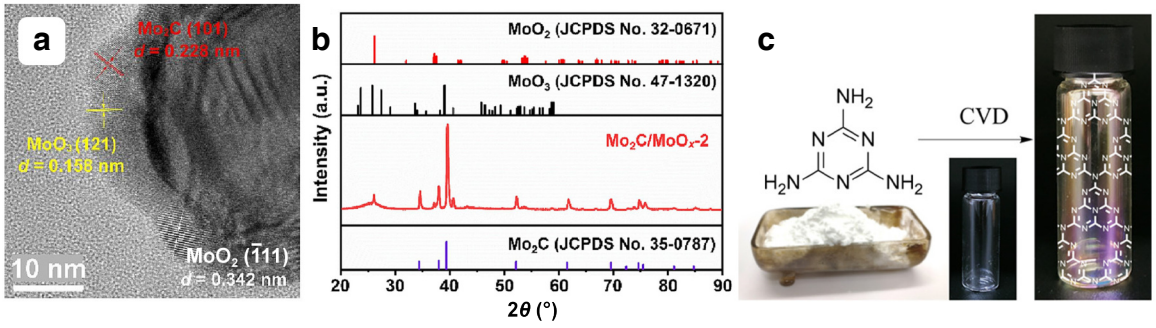

Fig. 2. **a**, HRTEM image of the Mo_2C/MoO_{x-2}. **b**, XRD patterns of the MoO_2, MoO_3, Mo_2C, and Mo_2C/MoO_{x-2}. Reproduced with permission from Ref.[36], © Elsevier B.V. 2023. **c**, Schematic of the CVD process of vial coating with CN. Reproduced with permission from Ref.[40], © Mazzanti, S. et al. 2021.

Giusto et al. employed a dual-zone CVD furnace, placing the melamine precursor in the first chamber and the substrate in the second[39]. Under vacuum, the substrate was initially heated to 550 °C, followed by heating the melamine to 300 °C. Nitrogen was used as the carrier gas to transport the evaporated precursor to the substrate, where it polymerized and deposited to form high-quality carbon nitride films. The films exhibited the highest inherent refractive index and transparency in the visible spectrum, paving the way for the manufacturing of devices in various related fields. Mazzanti et al. used CVD to deposited a carbon nitride films onto a common laboratory serum bottle (Fig. 2c), creating a reusable reactor that was applied to the oxidation of various aromatic alcohols with good conversion and selectivity for multiple substrates[40]. This work not only demonstrates the advantage of CVD in coating substrates with complex geometries but also introduces a novel approach to heterogeneous photocatalysis, eliminating the need for time-consuming post-reaction separation steps, such as filtration or centrifugation. This strategy expands the potential for scaling up photocatalytic reactions.

Although CVD offers significant advantages for deposition of films, its dependence on continuous gas-phase reactions imposes several inherent limitations. First, process control relies on multiple interdependent parameters, including precursor concentration, gas flow rate, and substrate temperature, making reproducible outcomes difficult to achieve without precise optimization. Second, the continuous nature of the deposition process renders sub-nanometer thickness control extremely challenging. Third, in high-aspect-ratio nanostructures, limited precursor diffusion into deep trenches or pores often results in non-uniform coverage and conformal coating deficiencies. These limitations, particularly the challenges associated with achieving extreme uniformity and atomic-scale precision, hinder large-scale production[41].

ALD is a powerful thin-film growth technique that enables atomic-scale thickness control. Unlike conventional methods, ALD grows films through sequential and self-limiting surface reactions achieved by alternately pulsing gaseous precursors into the reaction chamber, where they chemisorb and react exclusively on the substrate surface[42]. Each deposition cycle typically adds precisely one monolayer, resulting in a linear relationship between film thickness and the number of cycles and enabling thickness control with sub-angstrom precision. For instance, Deshpande et al. leveraged ALD to fabricate highly uniform TiO_2 and ZnO thin films with precisely controlled thicknesses ranging from 25 to 100 nm[43]. Their study revealed a non-monotonic relationship between films thickness and ultraviolet (UV)-induced superhydrophilicity in these metal oxides. By systematically investigating light absorption and charge-carrier transport, they identified optimal thicknesses, approximately 35 nm for TiO_2 and 75 nm for ZnO under 365 nm UV illumination, that maximize photoinduced hydrophilicity. This work highlights ALD as a versatile and precise tool for optimizing the thickness-dependent photocatalytic performance of thin-films materials.

Additionally, because ALD relies on sequential and self-limiting surface reactions, precursor molecules can access and uniformly coat any exposed surface irrespective of line-of-sight limitations. This unique attribute enables highly conformal deposition on complex three-dimensional structures, including high-aspect-ratio features, porous networks, and irregularly shaped substrates. Moreover, precise control over precursor selection, pulsing sequence, and cycle numbers allows atomic-level tailoring of films composition and uniform incorporation of dopants throughout the entire coated volume.

Zhang et al. demonstrated this capability by depositing ultrathin and conformal TiO_2 coatings onto commercial porous ceramic filter membranes using ALD[44]. By substituting NH_4OH for the conventional H_2O co-reactant, they successfully introduced nitrogen doping into the TiO_2 lattice, yielding N-doped TiO_2 without compromising the underlying porous structure. Scanning electron microscopy (SEM) images revealed negligible changes in surface morphology (**Figs.** 3a–3c), while energy dispersive X-ray (EDX) mapping confirmed homogeneous nitrogen distribution across the surface and deep within the pores (Figs. 3d and 3e). X-ray photoelectron spectroscopy (XPS) verified the formation of Ti–N bonds (Figs. 3f and 3g), and UV–visible (UV–vis) spectroscopy showed a clear red shift of the absorption edge (Figs. 3h and 3i). Consequently, the N-doped films exhibited strong visible-light photocatalytic activity and superior self-cleaning performance compared to their undoped counterparts. This example illustrates how ALD overcomes the inherent limitations of traditional coating techniques, such as non-uniform coverage and pore clogging, while preserving substrate architecture and imparting enhanced functionality.

Undoubtedly, the exceptional precision and conformality of ALD come at the cost of deposition rate. With typical growth rates of only 0.1–0.2 nm per cycle, fabricating thick films (> 100 nm) via ALD is both time-intensive and economically prohibitive. Nevertheless, the historical evolution from PVD to CVD, and ultimately to ALD, clearly reflects the community of the research relentless pursuit of superior uniformity, adhesion, conformality, and interfacial control in photocatalytic thin films. At the same time, the inherent drawbacks of vapor-phase techniques, particularly their dependence on vacuum systems and relatively high operational costs, have prompted parallel efforts to develop cost-effective and scalable alternatives. This has driven increasing

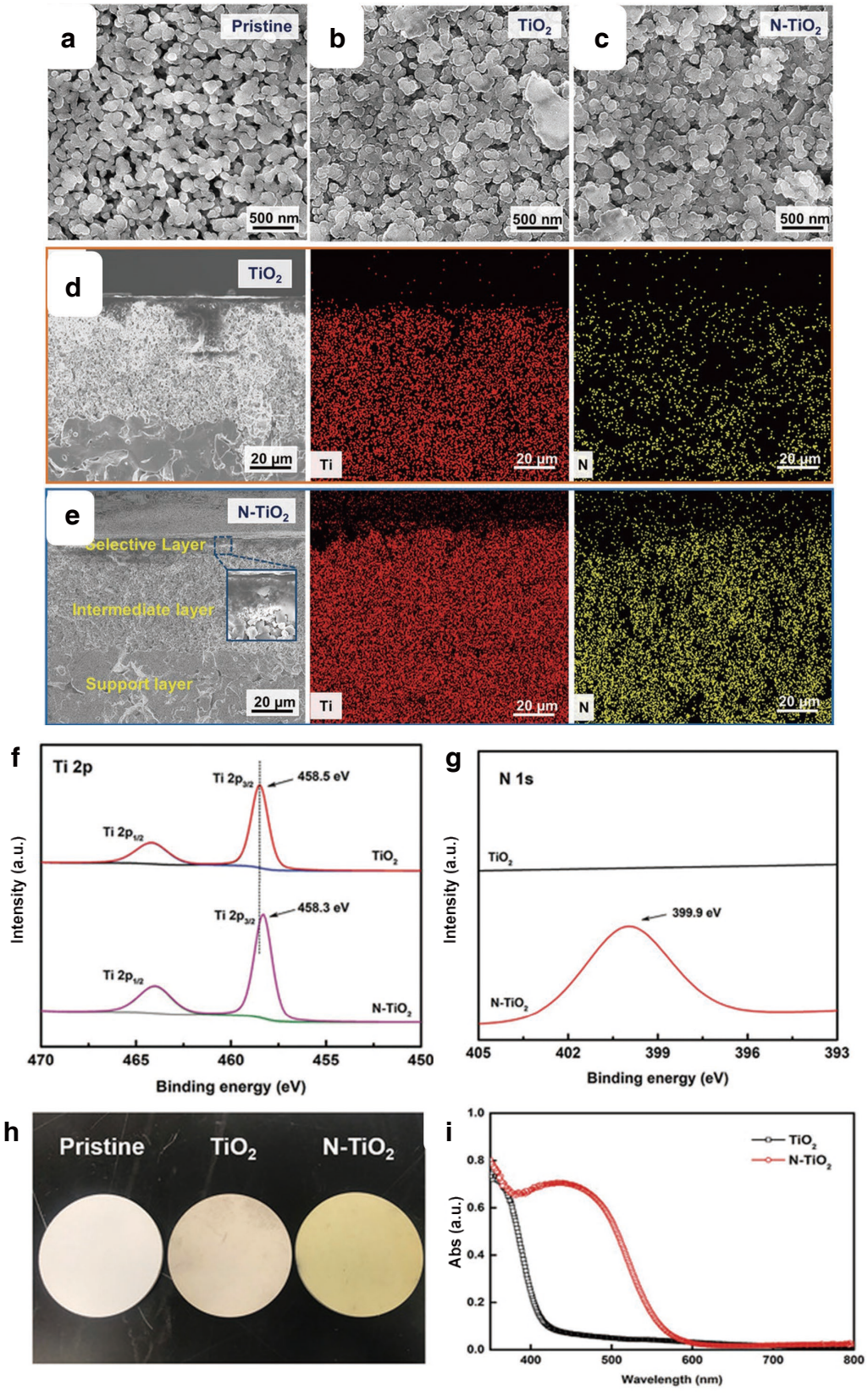

Fig. 3. **a**–**c**, The top-views of SEM images of the pristine (a), TiO_2 (b), and N-doped TiO_2-coated films (c). **d**, **e**, EDX mapping of the cross-section views of the membranes with TiO_2 (d) and N-TiO_2 ALD coating (e), respectively, showing significantly higher nitrogen content in the doped material. From the cross-section views, we can see the hierarchical structure of the membrane with a selective layer of ~ 5 μm, a intermediate layer of 50 μm, and the support layer (membrane thickness is 2.5 mm). **f**, **g**, XPS spectra for Ti (2p) (f) and N (1s) (g) signals of pure TiO_2 and N-doped TiO_2 films. **h**, Digital pictures of membranes before and after ALD modification. **i**, UV–vis absorption spectra of TiO_2 and N-doped TiO_2. Reproduced with permission from Ref.[44], © WILEY-VCH Verlag GmbH & Co. KGaA, Weinheim 2020.

interest in solution-based approaches that enable precise films growth under ambient or mild conditions while retaining many of the structural and compositional advantages of ALD.

2.4 Hydrothermal/solvothermal synthesis

Hydrothermal and solvothermal synthesis represent powerful solution-based routes for directly growing photocatalytic thin films on substrates inside sealed autoclaves, using water or organic solvents as the reaction medium[45]. These techniques rely on elevated temperature and autogenous pressure to dissolve precursors, followed by *in-situ* nucleation and crystallization directly on the substrate surface. In contrast to physical coating methods, hydrothermal/solvothermal growth forms strong chemical bonds between the films and substrate, significantly enhancing adhesion. Compared with energy-intensive vapor-phase techniques, they offer controllable nanostructure evolution under relatively mild and non-vacuum conditions. A key advantage is the exceptional tunability of reaction parameters (temperature, pressure, pH, precursor concentration, additives, and reaction time), which enables precise engineering of crystallographic orientation, crystal facet exposure, microstructure, and macroscopic films architecture. This integrated morphological and structural control provides an ideal platform for simultaneously optimizing light harvesting, photogenerated charge separation, and surface redox reactions in photocatalytic systems.

Thanks to its excellent control over crystallization kinetics, achieved through precise adjustment of solution pH, addition of mineralizers, capping agents, or surfactants, hydrothermal/solvothermal synthesis is particularly well suited for fabricating anisotropic nanostructures and highly ordered and vertically aligned architectures on substrates. For example, Hamed et al. employed a one-pot hydrothermal route to deposit nitrogen-doped TiO_2 films directly onto fluorine-doped tin oxide (FTO) substrates using titanium butoxide as the precursor[46]. The resulting films exhibited a hierarchical flower-like morphology composed of densely packed nanorods. In this system, triethylamine played a dual role: It served as the nitrogen source for doping while simultaneously acting as a facet-selective capping agent. By preferentially adsorbing onto the {110} facets of rutile TiO_2, triethylamine suppressed lateral growth, promoted elongation along the {110} direction, and ultimately directed the self-assembly of nanorods into the observed three-dimensional flower-like superstructures. This elegant strategy demonstrates how simple molecular additives can simultaneously achieve dopant incorporation and precise morphological control in a single hydrothermal step.

Chen et al. demonstrated the controlled hydrothermal growth of highly ordered rutile TiO_2 nanorod arrays directly on FTO substrates[47]. In their study, hydrochloric acid acted as a structural orientation agent during crystal growth: Cl^- ions selectively adsorbed onto the {110} side facets of rutile TiO_2, effectively suppressing lateral growth while promoting elongation along the {110} direction. This anisotropic growth led to the formation of nanorods with high aspect ratios. Moreover, the tetragonal crystal structure of the FTO substrate provided favorable lattice matching with rutile TiO_2, facilitating epitaxial nucleation and vertical alignment of the nanorods, which resulted in a well-aligned array structure. By employing multi-step hydrothermal processes, incorporating specific additives, or leveraging the self-assembly behavior of selected precursors, more complex three-dimensional hierarchical or porous architectures can be designed.

Wang et al. fabricated TiO_2 nanorod arrays on FTO substrates via hydrothermal treatment of tetrabutyl titanate, using HCl as a structure-directing agent[48]. Subsequently, $BiVO_4$ was hydrothermally deposited onto the TiO_2 nanorods using $Bi(NO_3)_3{\cdot}5H_2O$ and NH_4VO_3 as precursors. $Bi_2S_3/BiVO_4/TiO_2$ (BVT) composite films were then synthesized through an *in-situ* hydrothermal reaction, in which thiourea acted as the sulfur source and the pre-deposited $BiVO_4$ served as the Bi source. For comparison, the *ex-situ* method synthesized BVT films were also prepared by introducing additional $Bi(NO_3)_3{\cdot}5H_2O$ along with thiourea. Characterization results indicated that the *in-situ* approach produced Bi_2S_3 nanobelts with strong interfacial bonding, resulting in enhanced photocurrent density, reduced charge transfer resistance, and higher carrier density. In contrast, the *ex-situ* method yielded Bi_2S_3 with a radially aggregated spherical morphology, which was less effective in improving the photoelectrochemical performance.

Li et al. developed a facile hydrothermal approach for growing NH_2-UiO-66 MOF films directly onto flexible polyethylene terephthalate (PET) textile substrates (**Fig. 4**)[49]. The *in-situ* growth and strong adhesion of the MOF particles were driven by hydrogen bonding between the amino groups on the MOF ligands and the carbonyl groups on the PET fiber surfaces. Trifluoroacetic acid was employed as a modulator to decelerate the crystallization process, thereby enhancing the uniformity and robustness of MOF attachment across the fiber surfaces. The resulting films exhibited efficient overall CO_2 photoreduction performance without the need for sacrificial agents and retained high catalytic activity even after 60 h of continuous operation. This low-cost, scalable, and flexible MOF-based PET films provide promising insights for the design and development of large-area and flexible photocatalytic devices.

In summary, hydrothermal and solvothermal methods have proven to be powerful strategies for fabricating high-performance photocatalytic films, primarily due to their ability to facilitate the direct growth of complex nanostructures in solution. However, hydrothermal and solvothermal methods face significant constraints from an industrialization perspective. The scalability is intrinsically limited by the volume of high-pressure reactors, which in turn restricts the batch size and processing capacity. The choice of solvent systems is often limited and expensive, toxic, or flammable media may be required, which complicates large-scale safe handling, recovery, and disposal efforts. Additionally, the prolonged reaction time and high energy consumption for heating and cooling further impact process efficiency and cost. Therefore, these restrictions have prompted increasing interest in alternative techniques that allow for precise and controllable films deposition under ambient temperature and pressure.

2.5 Electrochemical deposition

Electrochemical deposition employs an external electric field to directly drive redox reactions at the surface of a conductive substrate, enabling the *in-situ* growth of thin films. This approach simplifies complex material synthesis into a potential- or current-controlled electrochemical process. By precisely programming electrical signals in a solution under ambient, the resulting films were formed. Due to its high controllability, low energy consumption, and minimal equipment requirements, electrochemical deposition is widely utilized in the fabrication of photoelectrodes[50]. Generally, this technique can be classified into two types: anodic oxidative deposition and cathodic reductive deposition[51,52].

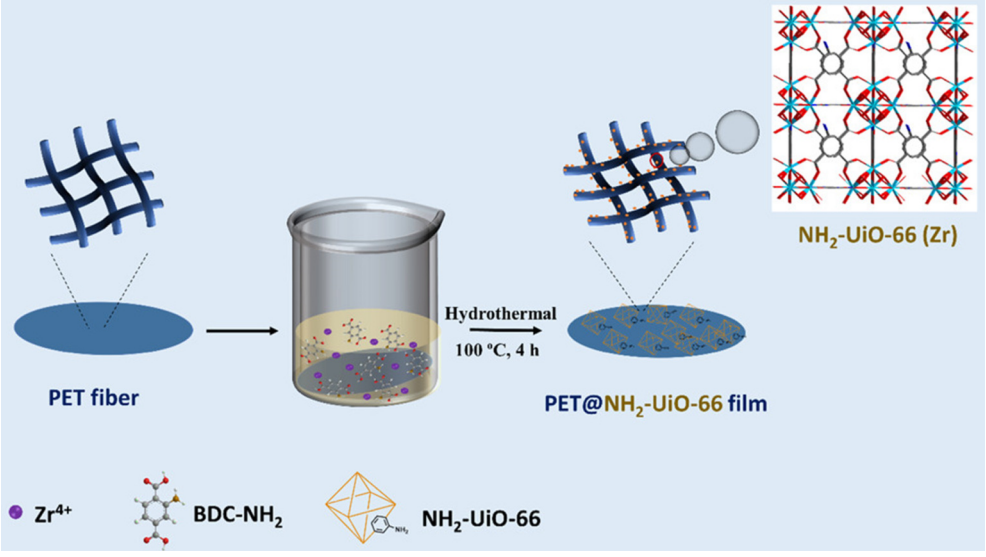

Fig. 4. Preparation approach of NH_2-UiO-66 particles on the PET fiber by a hydrothermal method. Reproduced with permission from Ref.[49], © American Chemical Society 2021.

For anodic processes, a recent study by Dippold et al. utilized cyclic voltammetry (CV) to deposit polymers onto a conductive FTO substrate, using 1,2,3,5-tetrakis(carbazol-9-yl)-4,6-dicyanobenzene (4CzIPN) as the precursor[53]. During anodic polarization, the carbazole groups in 4CzIPN undergo oxidation, losing electrons to form cationic radicals. These radicals subsequently participated in coupling reactions to form C–C bonds, leading to the *in-situ* polymerization and the growth of insoluble polymer films directly on the electrode surface. The thickness of the polymer films could be precisely controlled by adjusting the number of CV cycles. Due to the high local concentration and limited diffusion of reactive species at the electrode surface when the oxidation potential was first applied, the reaction was confined to an ultrathin region at the electrode–solution interface. Additionally, the electrode surface served as an anchoring site, enabling polymerization to proceed preferentially and controllably at the interface. This suppresses homogeneous nucleation in the bulk solution, highlighting a key advantage of the electrochemical approach for the preparation of functional polymer films. The resulting films were evaluated for photocatalytic hydrogen evolution under visible light irradiation (λ > 400 nm) with triethanolamine as a sacrificial agent. The films exhibited a surface-normalized activity of 703 $\mu mol \cdot m^{-2} \cdot h^{-1}$ and maintained stable performance over six catalytic cycles for 18 h. Further investigations explored the growth of semiconducting polymer films on FTO glass substrates patterned with micrometer-scale trenches. Electro-polymerization on these structured surfaces resulted in polymer films with vertical sidewalls and well-defined microstructures. This strategy reduced polymer consumption by 18% while maintaining the same area-normalized photocatalytic activity as unpatterned films, offering a promising route toward the design of spatially efficient and material-saving photocatalytic devices.

For the cathodic process, Wu et al. developed $BiVO_4$ photoanodes via an electrodeposition strategy[54]. The precursor solution was prepared by dissolving $Bi(NO_3)_3 \cdot 5H_2O$ and KI in aqueous nitric acid (pH 1.7), followed by mixing with an ethanol solution of p-benzoquinone. Under cathodic bias, p-benzoquinone was electrochemically reduced to hydroquinone, which increased the local pH near the electrode surface, thereby inducing the precipitation of crystalline BiOI. The resulting BiOI films was then treated with a dimethyl sulfoxide (DMSO) solution of vanadyl acetylacetonate via drop-casting and subsequently calcined in air to convert it into a $BiVO_4$ films. A cobalt porphyrin cocatalyst was electrodeposited onto the $BiVO_4$ surface to form a hybrid photoanode, referred to as BVCP. This photoanode demonstrated high efficiency in catalyzing the selective oxidation of styrene to 2-phenyloxirane under 495 nm LED illumination, achieving excellent conversion and selectivity for styrene and a variety of other olefin substrates. To evaluate the scalability, two types of scale-up experiments were conducted. First, the reaction volume was increased from the standard 10 to 90 mL. Under these conditions, the photocurrent remained stable over 40 h, yielding 0.3 g of the desired product, demonstrating excellent operational stability and the potential for gram-scale synthesis. Second, a large-area $BiVO_4$ films were fabricated by electrodepositing on a 10 cm × 10 cm FTO substrate using the same method.

However, for large-area electrodes, non-uniform voltage or current distribution, arising from internal resistance (Ohmic drop) within the electrode and the electrolyte, can hinder uniformity of films. To address this, the inclination angle of the electrode was adjusted during deposition to modulate the local Ohmic drop of electrolyte. At an optimal inclination angle of 30°, the current density distribution across the electrode was significantly improved, resulting in more uniform thin-films deposition (**Figs. 5**a–5c). This work provides valuable insights into scaling up photocatalytic films preparation via electrodeposition and highlights practical strategies for improving uniformity and performance in large-area photoelectrodes.

2.6 Electrospinning

Electrospinning is a technique that uses a high-voltage electrostatic field to physically stretch, refine, and solidify polymer solutions or melts, enabling the continuous production of ultrafine fibers. Although an electric field is applied, the core of electrospinning lies in the physical spinning process rather than electrodeposition on a substrate. During electrospinning, a high voltage creates a strong electrostatic field between the spinneret and the collector. The

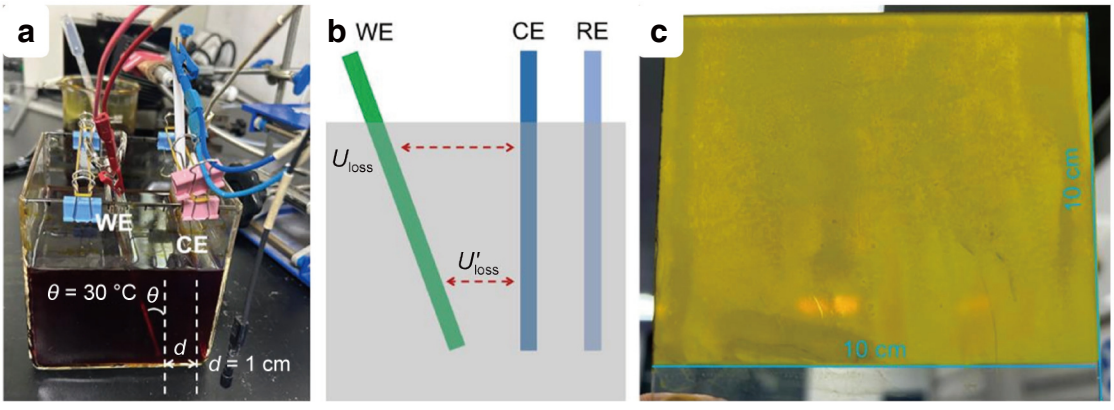

Fig. 5. **a**, Photo of preparation of large-area electrode sheets (bottom spacing "*d*" is 1 cm, and tilt angle "*θ*" is 30°). **b**, Schematic diagram of the working principle (U_{loss} and U'_{loss} are the Ohmic drops of the working electrode and the solution respectively). **c**, Macroscopic image of $BiVO_4$ precursor films. Reproduced with permission from Ref.[54], © Wiley-VCH GmbH 2024.

polymer droplet at the spinneret becomes charged, accumulating the same type of charges that generate strong Coulombic repulsion. Initially, surface tension holds the droplet at the tip in a hemispherical shape. As the electric field intensifies, the combined effect of Coulombic repulsion and electrostatic attraction eventually overcomes the surface tension of the droplets, stretching it into a stable cone pointing toward the collector. A fine and charged primary jet is ejected from the cone tip. As it travels toward the collector, the jet, loaded with like charges, undergoes vigorous whipping due to strong Coulombic repulsion, which rapidly stretches and thins it from micro- to nano-scale. During this flight, the solvent evaporates, resulting in the deposition of dried/cured ultrafine fibers in either a random or aligned manner on the collector.

In 2024, Chen et al. utilized a direct spinning-calcination method to fabricate fully inorganic Bi_2WO_6 (BWO) fibrous films[56]. Using polyvinyl pyrrolidone (PVP) as the structural template along with $Bi(NO_3)_3{\cdot}5H_2O$ and WCl_6 as the Bi and W precursors, they initially fabricated corresponding nanofiber precursors through electrospinning. These precursors were subsequently subjected to high-temperature calcination in air, leading to the decomposition of PVP and the formation of the final inorganic structure. By adjusting the calcination temperature and PVP content, the interpenetrating network structure of one-dimensional (1D) nanofibers and 2D nanosheets in the BWO films could be precisely tuned. As a result, the films rapidly degraded 100% of acetaldehyde under visible light and maintained this performance over 8 cycles without any decay.

Li et al. prepared PVDF/CSP films for photocatalytic hydrogen evolution by electrospinning a polymer solution containing PVDF and CdS@SiO_2-Pt photocatalyst, which was obtained by first synthesizing CdS nanorods (NRs) hydrothermally, then coating them with a SiO_2 shell using tetraethoxysilane to form core–shell CdS@SiO_2 NRs, and finally depositing Pt via impregnation[55]. The membrane exhibited high stability, enduring long-term mechanical stress from fluid flow and bubble collision while maintaining excellent performance in 50 cycles. Furthermore, when integrated into a flat-panel photocatalytic reactor, the membrane enabled efficient water splitting under strong outdoor solar illumination (**Figs. 6**a and 6b). Currently, although most highly performance powder photocatalysts for photocatalytic overall water splitting typically rely on drop–cast methods to fabricate photocatalytic panel reactors when moving toward scale-up, this study offers an alternative strategy for translating high-performance powder photocatalysts into functional panel-type photocatalytic devices.

Recently, Huang et al. synthesized the organic conjugated polymer photocatalyst Cz-AQ using phenylalkoxy-modified carbazole (Cz) and anthraquinone (AQ) as precursors. Subsequently, Cz-AQ was blended with polystyrene (PS) and polyacrylonitrile (PAN) to form a spinning solution, from which a self-standing flexible films, namely PF-Cz-AQ, was fabricated via electrospinning[57]. Unlike common single-polymer systems such as PVDF or PVP, this dual-component design allowed the hydrophilic/hydrophobic balance of the membrane to be tuned by adjusting the ratio of hydrophobic PS to hydrophilic PAN. Moreover, the films exhibitd a low density of ca. 4 mg·cm^{-2}, was self-floating, and naturally remained at the water–air interface, thereby maximizing light utilization and gas–liquid contact. The PF-Cz-AQ films were applied to photocatalytic water disinfection. Under natural cloudy-sky light, it achieved efficient bacterial inactivation in 10 L of highly contaminated water within 40 min, with no performance decay over 50 reuse cycles. Furthermore, the films performed effectively under various low-power household light sources such as desk lamps and mobile phone flashs, demonstrating strong potential for practical applications (Figs. 6c–6f).

Despite the challenges associated with mass production and precise control, electrospinning technology offers unique advantages for advancing photocatalytic applications. It enables the creation of a novel material form, self-supporting three-dimensional nanofiber films, breaking away from the traditional approach of growing or depositing thin films on substrates.

2.7 *In-situ* polymerization technology

In recent years, organic polymer semiconductors have been extensively studied in the field of photocatalytic solar fuel conversion due to their attractive features, including strong visible-light absorption, molecular-level tunability, high surface area offering abundant active sites, good biocompatibility, environmental friendliness, and low cost[58, 59]. Powder-based organic polymer photocatalysts have demonstrated excellent performance in various reactions, such as overall water splitting[60–62], CO_2 reduction[63–65], and organosynthesis[37, 66].

On the path toward scale-up, unlike inorganic semiconductors, organic polymer semiconductors possess highly extended conjugated network structures. If they are first prepared as powders and subsequently coated, the integrity of their conjugated networks

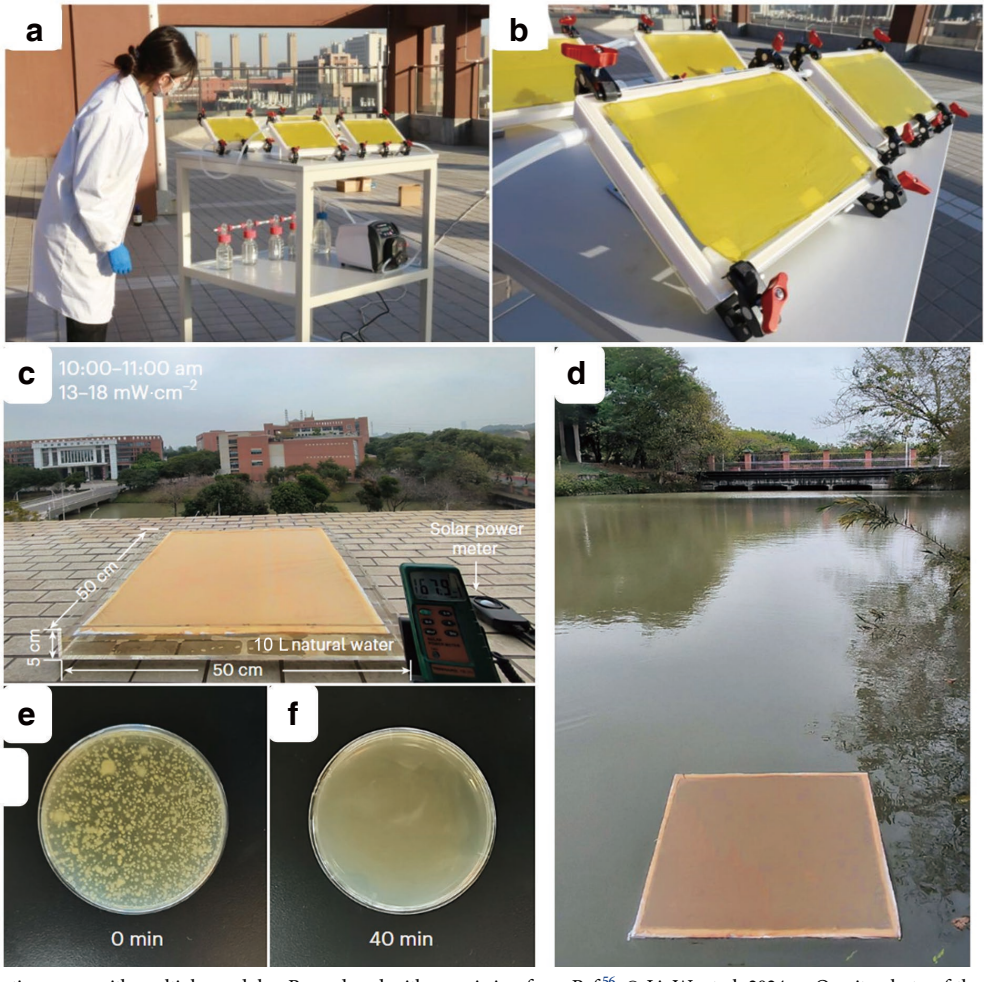

Fig. 6. **a**, **b**, Panel reaction array with multiple modules. Reproduced with permission from Ref.[56], © Li, W. et al. 2024. **c**, On-site photo of the experiment. **d**, Digital image of PF-CzAQ deployed in the Guhe River flowing through Sun Yat-sen University for *in-situ* purification. **e**, Photo of plate count agar of water before treatment. **f**, Photo of plate count agar of water after 40 min of treatment. Reproduced with permission from Ref.[57], © Huang, Y. Y. et al. 2025.

is inevitably compromised, leading to disruption of long-range charge-transport pathways, blockage of ordered pores, and a significant reduction of active interfaces, thereby severely diminishing their performance advantages. Consequently, *in-situ* polymerization has emerged as a more advanced and intrinsic thin-film fabrication strategy: It directly assembles molecular monomers "bottom-up" into continuous and covalently linked polymer films on substrate surfaces through precisely controlled chemical reactions. This approach not only fully preserves the designed molecular structure and functionality of the material, but also achieves robust chemical bonding between the films and the substrate.

For covalent organic frameworks (COFs), Liu et al. prepared TAPB-DMTA COF films through *in-situ* polymerization on a sapphire-supported monolayer MoS_2 substrate recently[67]. Using 1,3,5-tris-(4-aminophenyl)benzene (TAPB) and 2,5-dimethoxyterephthalaldehyde (DMTA) as monomers, the films were formed via Schiff-base condensation catalyzed by acetic acid. In this work, sapphire-supported monolayer MoS_2 films and SiO_2/Si substrates were used as controls. It was found that the atomically flat surface of the MoS_2 substrate exhibited van der Waals interactions with the COF precursors. These precursors and polymer fragments adsorbed on the surface and aligned orderly along the in-plane direction, guiding the COF to grow with its *ab*-plane parallel to the substrate, thereby forming a highly oriented films. Atomic force microscopy (AFM) measurements revealed that the films grown on the MoS_2 substrate showed significantly lower surface roughness compared to that grown on the SiO_2/Si substrate (**Figs.** 7a–7c). The TAPB-DMTA COF films were applied to the photocatalytic H_2O_2 generation, exhibiting a production rate of 8154 μmol·g^{-1}·h^{-1}. This activity was significantly higher than that of the powder form and of films grown on SiO_2/Si substrates, which was attributed to the formation of a COF/MoS_2 p–n heterojunction during growth. This research opens a new pathway for the rational design and device integration of COF films.

CTFs represent a distinctive class of covalent organic frameworks, characterized using triazine rings as their building blocks and a backbone rich in aromatic C=N double bond. This architectural design endows CTFs with remarkable chemical, physical, and thermal stability. In 2021, Hu et al. designed an imine precursor insoluble in DMSO, formed from the reaction of terephthalaldehyde and n-hexylamine[68]. This precursor was then floated on the surface of a DMSO solution containing terephthalamidine dihydrochloride and cesium carbonate. Upon heating to 60 °C, the imine precursor hydrolyzes and releases the aldehyde monomer. After reacting at 100 °C for 72 h, a continuous CTF films was formed via polymerization at the liquid–liquid interface. The lateral size of the films reached up to 250 cm^2, and its

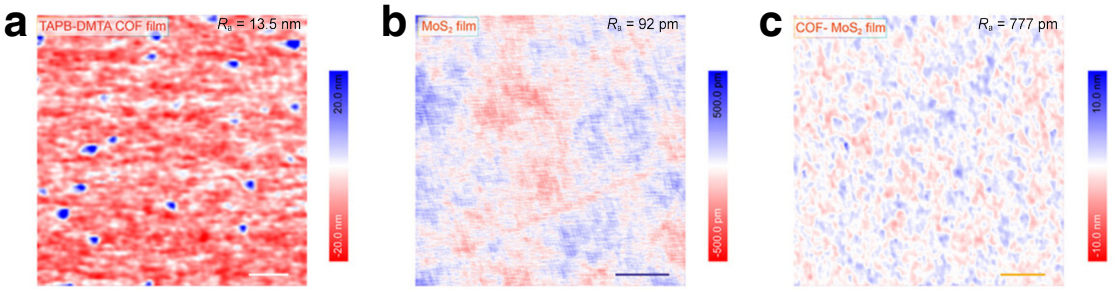

Fig. 7. **a**, AFM image of a COF films grown on a SiO_2/Si substrate. **b**, AFM image of single-layer MoS_2. **c**, AFM image of a COF films grown on a MoS_2 substrate. Scale bar: 1 μm in (a–c). Reproduced with permission from ref.[67], © Liu, M. H. et al. 2025.

thickness could be precisely tuned between 30 and 500 nm by adjusting the monomer concentration. The films exhibited self-supporting behavior, transparency, and flexibility, allowing for easy transfer and integration into devices. In this work, the films were directly fixed onto a glass slide to construct a simple photocatalytic device, which maintained good stability over 100 h of operation. This strategy, designing a solvent-insoluble precursor that spreads on the solvent surface to form an interface and guide interfacial polymerization, can be extended to other COF systems, offering a feasible fabrication route for developing photocatalytic thin-films devices.

Since the discovery in 2009 that polymeric carbon nitride (PCN) could be used for photocatalytic hydrogen production from water, research on carbon nitride photocatalysts has remained highly active[5]. Fang et al. prepared carbon nitride photoanode films by mixing different sulfur-containing precursors such as trithiocyanuric acid (TA), thiourea (TU), and thiosemicarbazide (TSC) and non-sulfur precursors melamine (M) or urea (U) in specific ratios. The blended powder was spread over cleaned FTO glass slides and calcined at 500 °C for 4 h under a nitrogen atmosphere to obtain the PCN films[69]. By varying the type and ratio of the precursors, 40 distinct PCN films morphologies were obtained. The results indicate that sulfur-containing precursors can form PCN islands, on which further polymerization is subsequently induced by non-sulfur precursors. In addition, XPS depth-profiling revealed that sulfur served as a molten medium during high-temperature treatment, promoting the nucleation and growth of PCN on the FTO surface (**Figs. 8**a–8d). It remains predominantly at the PCN–FTO interface, where it forms Sn–S bonds, thereby enhancing both the interfacial adhesion and charge-transport capability. The films prepared by this method achieved a PEC efficiency of approximately 100 μA·cm^{-2} (at 1.23 V_{RHE}) under AM 1.5G illumination in a NaOH electrolyte without any sacrificial agent, representing a significant improvement over contemporaneous PCN films.

Nonetheless, due to factors such as the relatively poor crystallinity of polymer semiconductors, their performance still lags considerably behind that of metal-oxide films. Building on this, Fang et al. further treated the sulfur-mediated PCN films by immersing them in concentrated phosphoric acid for low-temperature phosphorylation[70]. Without altering the fundamental physical and chemical properties of the films, such as their morphology and crystallinity, phosphate ions anchored onto defect sites on the PCN surface via ionic bonding. Acting as strong electron donors, these ions significantly increased the valence-band electron density at the film surface, thereby enhancing the kinetics of the water oxidation reaction. Furthermore, in terms of improving reaction kinetics, a method was reported involving the use of a precursor mixture of melamine and ammonium thiocyanate in varying ratios[71]. This mixture was first pre-polymerized at 300 °C for 1 h, followed by polymerization at 500 °C for 4 h, yielding a PCN films with a sulfur content that progressively increased along the films's thickness direction. In this case, by adjusting the precursor ratio, a non-uniform gradient doping of sulfur concentration from the bottom to the top of the films was achieved. This created a built-in electric field within the films, promoting charge separation and transport. Concurrently, sulfur doping gradually reduced the band gap from 2.80 to 2.55 eV, thereby broadening the material's visible light absorption.

In 2022, Li et al. mixed and ground melamine, thiourea, and $CoCl_2{\cdot}6H_2O$ in a specific ratio to obtain a light-blue precursor powder[72]. A clean FTO glass was then placed at the bottom of a crucible and covered with the precursor powder. Under a nitrogen atmosphere, the temperature was raised to 500 °C at a ramp rate of 2.3 °C·min^{-1} and held for 4 h, allowing the precursor to melt and polymerize on the FTO surface, thereby producing a CoS_2-merged polymeric carbon nitride films (CSCN). The introduction of CoS_2 not only promotes the formation of a nanosheet-like structure in PCN, increasing its specific surface area, but also, owing to its metallic-like conductivity, CoS_2 acts as a conductive layer that significantly reduces interfacial resistance. Serving as an electron-extraction and transport channel, it accelerates the transfer of photogenerated electrons to the FTO substrate, ultimately delivering a high PEC performance of 200 μA·cm^{-2} (at 1.23 V_{RHE}).

In the same year, Fan et al. predeposited a Ti layer approximately 25 nm thick onto an FTO substrate via magnetron sputtering. Subsequently, the precursor dicyandiamide was uniformly coated onto the Ti-FTO substrate. The temperature was then raised to 250 °C to melt the dicyandiamide into a uniform precursor films, followed by further heating to 550 °C under an Ar atmosphere to carry out thermal condensation, thereby forming PCN films[73]. During the high-temperature process, N→Ti coordination bonds formed between the sp^2-hybridized nitrogen in PCN and the Ti atoms, significantly enhancing the interfacial adhesion between the films and the substrate.

In a refreshing development, Battula et al. introduced a simple sandwich method for growing carbon nitride films on glass substrates in 2024[74]. In this approach, melamine and cyanuric acid were mixed in a specific ratio to form a supramolecular aggregate (melamine-cyanuric acid (MCA)). The MCA powder was then sandwiched between two glass substrates, creating a "glass/MCA/glass" layered structure. Upon calcination under a nitrogen atmosphere, the MCA polymerized *in-situ* on the glass surfaces into PCN films; after cooling, two uniformly coated PCN panels were obtained. Moreover, building on this method, a doctor-blade-assisted variation was developed. Here, MCA was dispersed

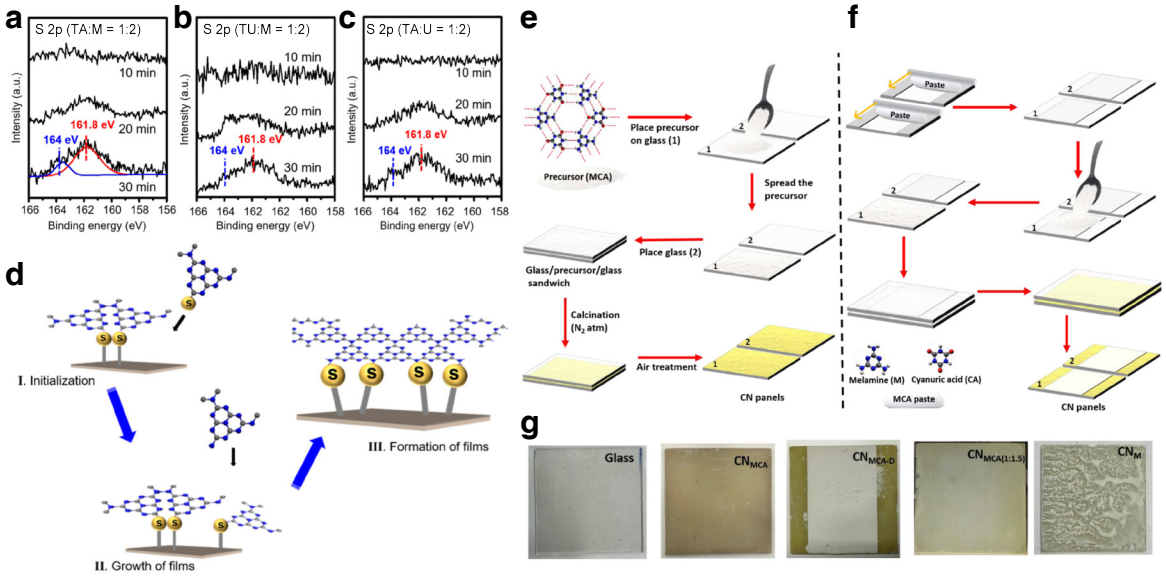

Fig. 8. **a–c**, Depth XPS study of the S 2p of the PCN films induced by TA/M = 1:2 (a), TU/M = 1:2 (b), and TA/U = 1:2 (c). **d**, The growth mechanism of the PCN using the mixture precursor. Reproduced with permission from Ref.[69], © American Chemical Society 2018. **e–g**, Schematic synthesis process of binder-free CN panels. "Sandwich" method using MCA supramolecular aggregates powder as the precursor (e), doctor-blade assisted "sandwich" method (f), and digital photos of a clean glass and CN panels (g). Reproduced with permission from Ref.[74], © American Chemical Society 2024.

in ethylene glycol to form a slurry, which was then blade-coated onto glass. After drying, the coated glass was again sandwiched with additional MCA powder and calcined, yielding thicker and more porous PCN panels (**Figs. 8e–8g**). These PCN panels were assembled into flat-panel photocatalytic reactors and demonstrated good activity and stability in various applications, including hydrogen peroxide production, organic pollutant degradation, water splitting for hydrogen evolution, and oxidation of 5-hydroxymethylfurfural. This strategy is straightforward, binder-free, and highly adaptable to diverse precursors and substrates, and holds significant promise for industrial-scale implementation.

In 2008, to achieve higher polymerization degree, extended conjugation, and improved crystallinity in polymeric carbon nitride, an ionothermal synthesis route for preparing crystalline carbon nitride was proposed[75]. Poly(heptazine imide), a crystalline carbon nitride based on heptazine units, has been extensively studied due to its larger π-conjugated system compared to triazine-based poly(triazine imide), endowing it with superior visible-light responsiveness. In 2022, Li et al. developed a novel method for fabricating highly crystalline potassium-poly(heptazine imide) (K-PHI) films via *in-situ* polymerization[76]. The K-PHI films were prepared by first pre-polymerizing melamine in air at 400 °C for 1 h to partially form a heptazine framework. The resulting powder was blended with ammonium thiocyanate in a defined ratio, placed over a cleaned FTO substrate in a crucible, and then calcined at 500 °C for 4 h under N_2. KSCN acts as a molten salt, whose low melting point enables it to melt during calcination, thereby enhancing heat and mass transfer within the reaction system. Consistent with earlier reports[69], the sulfur source in the system formed a SnS_2 layer on the FTO surface, which served as a seed for the growth of K-PHI crystals. Simultaneously, K^+ ions were intercalated into the heptazine-based framework, improving the stability of the crystalline structure. Driven by these combined effects, a highly crystalline K-PHI film was successfully fabricated. Owing to its markedly improved crystallinity relative to earlier amorphous melon-based films, this film delivered a photocurrent density of 800 μA·cm^{-2} under AM 1.5G illumination without sacrificial agents. This performance corresponds to about a 20-fold enhancement compared to the amorphous melon films.

Building on this work, Su et al. further optimized the molten-salt system in 2024. The K-PHI films were prepared using the same method, during which NH_4SCN and K_2CO_3 were introduced as binary molten salts[77]. This work first proposed a binary molten-salt system consisting of NH_4SCN and K_2CO_3, where NH_4SCN modulates seed-layer formation while K_2CO_3 tunes crystallinity, thereby resolving the compromise inherent in using a single molten salt. Furthermore, NH_4SCN and K_2CO_3 are less corrosive to the substrate than KSCN, which helps retain the substrate's conductivity. This approach offers a new strategy for designing and fabricating polymer photoanodes.

In summary, *in-situ* polymerization presents an ideal strategy for fabricating high-performance polymeric semiconductor photocatalytic thin films. Although goals such as improving films-substrate adhesion and controlling films structure and thickness have been partially achieved through various regulatory methods, challenges remain in scaling up for practical applications. These challenges include the relatively low intrinsic conductivity of polymeric semiconductors and the absence of reliable methods for producing large-area, uniform, and highly crystalline films.

3 Conclusions and perspective

Over the past three decades, the development of photocatalytic thin films for scalable solar fuel production has been an ongoing pursuit. From traditional coating and casting methods to advanced techniques such as PVD, CVD, hydrothermal synthesis, electrospinning, and, more recently, *in-situ* polymerization, progress has been made in advancing thin-films fabrication technologies (**Table 1**). These efforts reflect a continuous drive to achieve precise structural control in scalable photocatalytic devices, ensure robust mechanical stability between films and substrates, and optimize process costs and workflows.

Table 1 Advantages and disadvantages of film preparation methods and their applications

Method	Bonding nature and mechanism	Advantages	Limitations	Application			
				Field	Scale (cm^2)	Performance	Ref.
Coating photocatalyst powder	van der Waals force	Simple operation and scalability	Weak interfacial bonding	Over water splitting	1,000,000	27.2 mol H_2 (1 day) STH: > 0.4% (> 1600 h)	[26]
Physical vapor deposition	High-energy particle bombardment (strong physical)	Excellent films properties and reproducible processing	Line-of-sight limitation and high cost	Methylene blue photodegradation	6.25	Apparent first-order rate constants: 0.0389 min^{-1}	[28]
Chemical vapor deposition	Chemical bond	High crystallinity, excellent conformity, and material range	Requires high temperature and precise control	H_2O_2 production	19.625	H_2O_2 production rate: 14.2 $mmol{\cdot}m^{-2}{\cdot}h^{-1}$	[38]
Atomic Layer deposition	Chemical bond	Atomic-level thickness control and superior interface quality	Slow growth rate and high cost	Self-cleaning membranes	17.34	Self-cleaning within 3 h after 0.5 $g{\cdot}L^{-1}$ bovine serum albumin (BSA) fouling	[44]
Hydrothermal/solvothermal synthesis	Chemical bond	Enables nanostructure engineering	High temperature, high pressure, and non-uniform on large area	Cr(VI) reduction	10	Degradation efficiency: 93.5% (100 min)	[48]
Electrochemical deposition	Chemical bond	Mild, controllable conditions, and simple setup	Limited material scope and non-uniform on large area	Alkene epoxidation	100	Conversion: 87% (gram-scale) Selectivity: 89%	[54]
Electrospinning	Self-supporting or van der Waals forces	Self-supporting, high surface area, and low cost	Moderate strength and low efficiency	Water disinfection	2500	10 L sewage treatment within 40 min (bacterial elimination)	[57]
In-situ polymerization technology	Chemical bond	Molecular-level tunability, superior interfacial chemical bonding, and structure integrity	Harsh synthesis conditions, limited to organic polymers, and low intrinsic carrier mobility of organic polymers	5-hydroxymethyfurfural oxidation to 2,5-diformylfuran	100	Conversion rate: 1185 $\mu mol{\cdot}g^{-1}{\cdot}h^{-1}$	[74]

These efforts reflect the relentless pursuit of precise structural control in scalable photocatalytic devices, robust mechanical stability between films and substrates, and the optimization of process costs and workflows. Currently, the dominant methods for fabricating devices aimed at large-scale photocatalytic solar fuel production remain coating and casting. Despite numerous technical improvements, the lack of effective bonding between the films material and the substrate continues to challenge the mechanical stability of the films, particularly when subjected to long-term fluid flow and bubble impact. Although PVD and ALD provide precise films control, they are limited by low production efficiency and high costs. Hydrothermal and electrodeposition methods show considerable potential in terms of cost and scalability, but issues such as uniformity and reproducibility must still be addressed. *In-situ* polymerization offers simple processing, low cost, and tunable films structures, but it is primarily applicable to organic polymer semiconductors and faces inherent challenges such as slow reaction kinetics.

Therefore, a practical and scalable fabrication technology for future photocatalytic devices should not rely on the extreme adoption of any single method, but rather integrate multiple techniques in a synergistic manner to compensate the limitations for each other. Organic polymer semiconductors, particularly polymeric carbon nitride, present a highly promising material for scalable solar fuel production. This potential arises from their effective use of the visible portion of the solar spectrum, structurally flexible and tunable frameworks, environmental friendliness, and low cost. Given the inherently slow reaction kinetics of carbon nitride, a promising strategy is to deposit suitable cocatalysts onto the as-formed carbon nitride films using techniques such as CVD or ALD. This approach aims to enhance reaction kinetics and ultimately achieve efficient and large-scale solar fuel production. To date, the largest example of practical photocatalytic application remains the 100 m^2 of $SrTiO_3$ solar panel, which marks a significant step toward practical application in photocatalysis. Inspired by this, this review explores the potential of this method to realize photocatalytic films and scale them up for large-scale applications.

References

[1] Wang, Q.; Warnan, J.; Rodríguez-Jiménez, S.; Leung, J. J.; Kalathil, S.; Andrei, V.; Domen, K.; Reisner, E. Molecularly engineered photocatalyst sheet for scalable solar formate production from carbon dioxide and water. *Nat. Energy* **2020**, *5*, 703–710.

[2] Fang, Y. X.; Zheng, Y.; Fang, T.; Chen, Y.; Zhu, Y. D.; Liang, Q.; Sheng, H.; Li, Z. S.; Chen, C. C.; Wang, X. C. Photocatalysis: An overview of recent developments and technological advancements. *Sci. China Chem.* **2020**, *63*, 149–181.

[3] Fujishima, A.; Honda, K. Electrochemical photolysis of water at a semiconductor electrode. *Nature* **1972**, *238*, 37–38.

[4] Takata, T.; Jiang, J. Z.; Sakata, Y.; Nakabayashi, M.; Shibata, N.; Nandal, V.; Seki, K.; Hisatomi, T.; Domen, K. Photocatalytic water splitting with a quantum efficiency of almost unity. *Nature* **2020**, *581*, 411–414.

[5] Wang, X. C.; Maeda, K.; Thomas, A.; Takanabe, K.; Xin, G.; Carlsson, J. M.; Domen, K.; Antonietti, M. A metal-free polymeric photocatalyst for hydrogen production from water under visible light. *Nat. Mater.* **2009**, *8*, 76–80.

[6] Wang, Q.; Zhang, G. G.; Xing, W. D.; Pan, Z. M.; Zheng, D. D.; Wang, S. B.; Hou, Y. D.; Wang, X. C. Bottom-up synthesis of single-crystalline poly(triazine imide) nanosheets for photocatalytic overall water splitting. *Angew. Chem., Int. Ed.* **2023**, *62*, e202307930.

[7] Yang, P. J.; Ou, H. H.; Fang, Y. X.; Wang, X. C. A facile steam reforming strategy to delaminate layered carbon nitride semiconductors for photoredox catalysis. *Angew. Chem., Int. Ed.* **2017**, *56*, 3992–3996.

[8] Ou, H. H.; Lin, L. H.; Zheng, Y.; Yang, P. J.; Fang, Y. X.; Wang, X. C. Tri-*s*-triazine-based crystalline carbon nitride nanosheets for an improved hydrogen evolution. *Adv. Mater.* **2017**, *29*, 1700008.

[9] Fang, Y. X.; Xu, Y. T.; Li, X. C.; Ma, Y. W.; Wang, X. C. Coating polymeric carbon nitride photoanodes on conductive Y:ZnO nanorod arrays for overall water splitting. *Angew. Chem., Int. Ed.* **2018**, *57*, 9749–9753.

[10] Luo, L. Y.; Wu, Q. L.; Wang, S. Y.; Song, H. J.; Li, J. Q.; Zhang, L. P.; Zhang, Q.; Fang, Y. X.; Jiang, B. J.; Wang, X. C. Defective poly(heptazine imide) nanosheets for efficient one-step two-electron photocatalytic O_2 reduction to medical-like H_2O_2. *Angew. Chem., Int. Ed.* **2025**, *64*, e202507415.

[11] Ou, H. H.; Chen, X. R.; Lin, L. H.; Fang, Y. X.; Wang, X. C. Biomimetic donor-acceptor motifs in conjugated polymers for promoting exciton splitting and charge separation. *Angew. Chem., Int. Ed.* **2018**, *57*, 8729–8733.

[12] Fang, Y. X.; Fu, X. Z.; Wang, X. C. Diverse polymeric carbon nitride-based semiconductors for photocatalysis and variations. *ACS Mater. Lett.* **2020**, *2*, 975–980.

[13] Tao, Y. L.; Li, S.; Zhao, S.; Li, D. W.; Wu, Y. N.; Liang, Z. Q.; Cheng, H. TiO_2/PANI/graphene-PVA hydrogel for recyclable and highly efficient photo-electrocatalysts. *Ind. Eng. Chem. Res.* **2021**, *60*, 10033–10043.

[14] Xu, X. L.; Wang, Y.; Zhang, D. A novel strategy of hydrothermal *in-situ* grown bismuth based film on epoxy resin as recyclable photocatalyst for photodegrading antibiotics and sterilizing microorganism. *Sep. Purif. Technol.* **2022**, *290*, 120842.

[15] Gopinath, C. S.; Nalajala, N. A scalable and thin film approach for solar hydrogen generation: A review on enhanced photocatalytic water splitting. *J. Mater. Chem. A* **2021**, *9*, 1353–1371.

[16] Hisatomi, T.; Domen, K. Reaction systems for solar hydrogen production via water splitting with particulate semiconductor photocatalysts. *Nat. Catal.* **2019**, *2*, 387–399.

[17] Takahashi, M.; Mita, K.; Toyuki, H.; Kume, M. Pt-TiO_2 thin films on glass substrates as efficient photocatalysts. *J. Mater. Sci.* **1989**, *24*, 243–246.

[18] Zuo, Q.; Liu, T. T.; Chen, C. S.; Ji, Y.; Gong, X. Q.; Mai, Y. Y.; Zhou, Y. F. Ultrathin metal-organic framework nanosheets with ultrahigh loading of single pt atoms for efficient visible-light-driven photocatalytic H_2 evolution. *Angew. Chem., Int. Ed.* **2019**, *58*, 10198–10203.

[19] Shi, X. W.; Dai, C.; Wang, X.; Hu, J. Y.; Zhang, J. Y.; Zheng, L. X.; Mao, L.; Zheng, H. J.; Zhu, M. S. Protruding Pt single-sites on hexagonal $ZnIn_2S_4$ to accelerate photocatalytic hydrogen evolution. *Nat. Commun.* **2022**, *13*, 1287.

[20] Wang, C. X.; Zhang, H. L.; Luo, W. J.; Sun, T.; Xu, Y. X. Ultrathin crystalline covalent-triazine-framework nanosheets with electron donor groups for synergistically enhanced photocatalytic water splitting. *Angew. Chem., Int. Ed.* **2021**, *60*, 25381–25390.

[21] Feng, Y. J.; Gong, S. K.; Wang, Y.; Ban, C. G.; Qu, X. L.; Ma, J. P.; Duan, Y. Y.; Lin, C.; Yu, D. M.; Xia, L. et al. Noble-metal-free cocatalysts reinforcing hole consumption for photocatalytic hydrogen evolution with ultrahigh apparent quantum efficiency. *Adv. Mater.* **2025**, *37*, 2412965.

[22] Wang, X.; Liu, B. Y.; Ma, S. Q.; Zhang, Y. J.; Wang, L. Z.; Zhu, G. Q.; Huang, W.; Wang, S. C. Induced dipole moments in amorphous ZnCdS catalysts facilitate photocatalytic H_2 evolution. *Nat. Commun.* **2024**, *15*, 2600.

[23] Valencia-Valero, L. C.; Simbaña, K. A.; Ruscigno, M.; Giamberini, M.; Hapońska, M.; Puga, A. Hydrogen production by solar photoreforming of urban wastewaters in thin-layer flat catalytic panels. *Adv. Funct. Mater.* **2025**, *35*, 2502903.

[24] Gu, C.; Miseki, Y.; Nishiyama, H.; Takata, T.; Yoshimura, J.; Ma, Y. W.; Lin, L. H.; Hisatomi, T.; Lu, D. L.; Zettsu, N. et al. Carbon-conductor-based photocatalyst sheets fabricated by a facile filtration process for efficient, stable, and scalable water splitting. *Chem Catal.* **2025**, *5*, 101233.

[25] Wang, Q.; Hisatomi, T.; Jia, Q. X.; Tokudome, H.; Zhong, M.; Wang, C. Z.; Pan, Z. H.; Takata, T.; Nakabayashi, M.; Shibata, N. et al. Scalable water splitting on particulate photocatalyst sheets with a solar-to-hydrogen energy conversion efficiency exceeding 1%. *Nat. Mater.* **2016**, *15*, 611–615.

[26] Nishiyama, H.; Yamada, T.; Nakabayashi, M.; Maehara, Y.; Yamaguchi, M.; Kuromiya, Y.; Nagatsuma, Y.; Tokudome, H.; Akiyama, S.; Watanabe, T. et al. Photocatalytic solar hydrogen production from water on a 100-m^2 scale. *Nature* **2021**, *598*, 304–307.

[27] Weinberger, B. R.; Garber, R. B. Titanium dioxide photocatalysts produced by reactive magnetron sputtering. *Appl. Phys. Lett.* **1995**, *66*, 2409–2411.

[28] Bonomi, S.; Galinetto, P.; Patrini, M.; Romani, L.; Malavasi, L. Optical and structural property tuning in physical vapor deposited bismuth halides $Cs_3Bi_2(I_{1-x}Br_x)_9$ ($0 \le x \le 1$). *Inorg. Chem.* **2021**, *60*, 14142–14150.

[29] Hui, Q.; Li, Q. K.; Wang, S.; Xue, J. S.; Zhou, Z. W.; Hu, Y. Q.; Zhou, Z.; Feng, Z. J.; Yan, Q. Y.; Zheng, F. G. et al. Highly efficient flexible $BiVO_4$ thin-film photodetector with good bending robustness on mica substrates. *J. Phys. Chem. C* **2023**, *127*, 18219–18226.

[30] Timoumi, A.; El Guesmi, N.; Alamri, S. N.; Alsalmi, O. H.; Ahmed, S. A. Constructing of novel Cu_2AlSnS_4 (CATS) compound: Synthesis, chracterization and photocatalytic activities approach. *J. Inorg. Organomet. Polym. Mater.* **2023**, *33*, 1592–1602.

[31] Ichihashi, Y.; Sekiguchi, T.; Tokui, Y.; Hori, R.; Naito, S.; Koshiba, Y.; Sutani, Y.; Ishida, K.; Taniya, K.; Nishiyama, S. Decomposition of water over picene derivatives photocatalyst under visible light irradiation. *Catal. Today* **2023**, *410*, 317–322.

[32] Kraut, M.; Sirotti, E.; Pantle, F.; Jiang, C. M.; Grötzner, G.; Koch, M.; Wagner, L. I.; Sharp, I. D.; Stutzmann, M. Control of band gap and band edge positions in gallium-zinc oxynitride grown by molecular beam epitaxy. *J. Phys. Chem. C* **2020**, *124*, 7668–7676.

[33] Byun, D.; Jin, Y.; Kim, B.; Lee, J. K.; Park, D. Photocatalytic TiO_2 deposition by chemical vapor deposition. *J. Hazard. Mater.* **2000**, *73*, 199–206.

[34] Liu, H. M.; Li, K. Z.; Chen, H.; Liu, B.; Yin, X. M. Facile growth of oriented SiC nanowires arrays on carbon fiber cloth via CVD. *Ceram. Int.* **2022**, *48*, 34543–34549.

[35] Liu, M. H.; Wei, C. G.; Zhuzhang, H. Y.; Zhou, J. M.; Pan, Z. M.; Lin, W.; Yu, Z. Y.; Zhang, G. G.; Wang, X. C. Fully condensed poly (triazine imide) crystals: Extended π-conjugation and structural defects for overall water splitting. *Angew. Chem., Int. Ed.* **2022**, *61*, e202113389.

[36] Lian, Z.; Wu, T.; Zhang, X. N.; Cai, S. F.; Xiong, Y. L.; Yang, R. Synergistic degradation of tetracycline from Mo_2C/MoO_x films mediated peroxymonosulfate activation and visible-light triggered photocatalysis. *Chem. Eng. J.* **2023**, *469*, 143774.

[37] Wang, Y.; Fang, Y. X.; Wang, Y. K.; Wu, H. S.; Anpo, M.; Yu, J. C.; Wang, X. C. Plasma-enhanced chemical-vapor-deposition synthesis of photoredox-active nitrogen-doped carbon from NH_3 and CH_4 gases. *Angew. Chem., Int. Ed.* **2023**, *62*, e202307236.

[38] Lei, B.; Tu, Z. X.; Chen, D.; Luo, Q.; Peng, X. Y.; Wu, S. Q.; Peng, G. M. Nitrogen-defective carbon nitride nanorod arrays for continuous-flow photosynthesis of H_2O_2. *Chin. Chem. Lett.*, in press, https://doi.org/10.1016/j.cclet.2025.112004.

[39] Giusto, P.; Cruz, D.; Heil, T.; Arazoe, H.; Lova, P.; Aida, T.; Comoretto, D.; Patrini, M.; Antonietti, M. Shine bright like a diamond: New light on an old polymeric semiconductor. *Adv. Mater.* **2020**, *32*, 1908140.

[40] Mazzanti, S.; Manfredi, G.; Barker, A. J.; Antonietti, M.; Savateev, A.; Giusto, P. Carbon nitride thin films as all-in-one technology for photocatalysis. *ACS Catal.* **2021**, *11*, 11109–11116.

[41] Kalanyan, B.; Lemaire, P. C.; Atanasov, S. E.; Ritz, M. J.; Parsons, G. N. Using hydrogen to expand the inherent substrate selectivity window during tungsten atomic layer deposition. *Chem. Mater.* **2016**, *28*, 117–126.

[42] Lee, J. P.; Kim, H. K.; Park, C. R.; Park, G.; Kwak, H. T.; Koo, S. M.; Sung, M. M. Photocatalytic decomposition of alkylsiloxane self-assembled monolayers on titanium oxide surfaces. *J. Phys. Chem. B* **2003**, *107*, 8997–9002.

[43] Deshpande, R. A.; Navne, J.; Adelmark, M. V.; Shkondin, E.; Crovetto, A.; Hansen, O.; Bachmann, J.; Taboryski, R. Understanding the light induced hydrophilicity of metal-oxide thin films. *Nat. Commun.* **2024**, *15*, 124.

[44] Zhang, H. R.; Mane, A. U.; Yang, X. B.; Xia, Z. J.; Barry, E. F.; Luo, J. Q.; Wan, Y. H.; Elam, J. W.; Darling, S. B. Visible-light-activated photocatalytic films toward self-cleaning membranes. *Adv. Funct. Mater.* **2020**, *30*, 2002847.

[45] Lee, S. H.; Kang, M.; Cho, S. M.; Han, G. Y.; Kim, B. W.; Yoon, K. J.; Chung, C. H. Synthesis of TiO_2 photocatalyst thin film by solvothermal method with a small amount of water and its photocatalytic performance. *J. Photochem. Photobiol. A* **2001**, *146*, 121–128.

[46] Hamed, N. K. A.; Nafarizal, N.; Ahmad, M. K.; Faridah, A. B.; Makhtar, S. N. N. M.; Noor, S. F. M.; Shimomura, M. Synergistic coupling {101}-{111} facet of N-doped TiO_2 film enhance spatial charge separation for methylene blue photodegradation. *J. Alloys Compd.* **2023**, *961*, 170977.

[47] Chen, C. L.; Wei, Y. L.; Yuan, G. Z.; Liu, Q. L.; Lu, R. R.; Huang, X.; Cao, Y.; Zhu, P. H. Synergistic effect of Si doping and heat treatments enhances the photoelectrochemical water oxidation performance of TiO_2 nanorod arrays. *Adv. Funct. Mater.* **2017**, *27*, 1701575.

[48] Wang, H. W.; Zhu, Y. W.; Kumar Joshi, M.; Cheng, Y.; Zhang, P. Y.; Tan, M. H.; Yu, R. H.; Mao, Z. P.; Li, X. L. *In-situ* and *ex-situ* preparation of Bi_2S_3 on the $BiVO_4/TiO_2$ to construct $Bi_2S_3/BiVO_4/TiO_2$ heterojunction for efficient Cr(VI) reduction. *Chem. Eng. J.* **2024**, *500*, 156640.

[49] Li, P. X.; Yan, X. Y.; Song, X. M.; Li, J. J.; Ren, B. H.; Gao, S. Y.; Cao, R. Zirconium-based metal-organic framework particle films for visible-light-driven efficient photoreduction of CO_2. *ACS Sustain. Chem. Eng.* **2021**, *9*, 2319–2325.

[50] Jiao, Y. Y.; Yang, B.; Li, T.; Song, Y. R.; Jiang, J. W.; Wang, C.; Jin, D. F.; Hu, Z. Q.; Jiao, S. Y.; Chen, G. H. et al. Photoelectrocatalytic upgrading of biomass derivatives for efficient C–N coupling with formamide. *J. Am. Chem. Soc.* **2025**, *147*, 31679–31688.

[51] Matsumoto, Y.; Ishikawa, Y.; Nishida, M.; Ii, S. A new electrochemical method to prepare mesoporous titanium(IV) oxide photocatalyst fixed on alumite substrate. *J. Phys. Chem. B* **2000**, *104*, 4204–4209.

[52] Song, Y. R.; Jiao, Y. Y.; Jiang, J. W.; Jiao, S. Y.; Hu, Z. Q.; Lu, S. J.; Chen, G. H.; Yang, B.; Feng, J. Y.; Hou, J. G. Chemically cross-linked conductive network hydrogel as dual-functional layer enabling stable solar water splitting. *ACS Nano* **2025**, *19*, 38067–38076.

[53] Dippold, V.; Küçükkeçeci, H.; Bosler, E.; Schmidt, J.; Ghosh, S.; Michl, G.; Khalil, I. E.; Gerland, L.; Lange, A.; Oberschmidt, D. et al. Carbazole-based thin microporous polymer films for photocatalytic hydrogen evolution. *Adv. Mater.* **2025**, *37*, 2506689.

[54] Wu, H. S.; Wang, Y. K.; Huang, M. R.; Cheng, J. J.; Sa, B. S.; Fang, Y. X.; Wang, X. C. Alkene epoxidation with water by confined active Co sites on $BiVO_4$ photoanodes under visible light. *Angew. Chem., Int. Ed.* **2025**, *64*, e202420188.

[55] Chen, Y. H.; Zhang, L.; Chen, S.; Sun, S. M.; Cheng, H.; Li, S. Z.; Yu, J. Y.; Ding, B.; Yan, J. H. Synthesis of heteromorphic Bi_2WO_6 films with an interpenetrate 1D/2D network structure for efficient and stable photocatalytic degradation of VOCs. *Adv. Mater.* **2024**, *36*, 2407400.

[56] Li, W.; Duan, W.; Liao, G. C.; Gao, F. F.; Wang, Y. S.; Cui, R. X.; Zhao, J. C.; Wang, C. Y. 0.68% of solar-to-hydrogen efficiency and high photostability of organic–inorganic membrane catalyst. *Nat. Commun.* **2024**, *15*, 6763.

[57] Huang, Y. Y.; Li, X. J.; Yan, H. J.; Xu, J. Q.; Zhu, F.; Ye, Y. X.; Ouyang, G. F. Reusable photocatalytic film for efficient water disinfection under low light intensity. *Nat. Water* **2025**, *3*, 1003–1016.

[58] Liu, L. J.; Gao, M. Y.; Yang, H. F.; Wang, X. Y.; Li, X. B.; Cooper, A. I. Linear conjugated polymers for solar-driven hydrogen peroxide production: The importance of catalyst stability. *J. Am. Chem. Soc.* **2021**, *143*, 19287–19293.

[59] Yang, H. F.; Li, C.; Liu, T.; Fellowes, T.; Chong, S. Y.; Catalano, L.; Bahri, M.; Zhang, W. W.; Xu, Y. J.; Liu, L. J. et al. Packing-induced selectivity switching in molecular nanoparticle photocatalysts for hydrogen and hydrogen peroxide production. *Nat. Nanotechnol.* **2023**, *18*, 307–315.

[60] Zhuzhang, H. Y.; Liang, X. C.; Li, J. X.; Xue, S. K.; Lin, Y. F.; Sa, B. S.; Wang, S. B.; Zhang, G. G.; Yu, Z. Y.; Wang, X. C. Precise manipulation on the structural defects of poly(triazine imide) single crystals for efficient photocatalytic overall water splitting. *Angew. Chem., Int. Ed.* **2025**, *64*, e202421861.

[61] Liu, M. H.; Zhang, G. G.; Liang, X. C.; Pan, Z. M.; Zheng, D. D.; Wang, S. B.; Yu, Z. Y.; Hou, Y. D.; Wang, X. C. Rh/Cr_2O_3 and CoO_x cocatalysts for efficient photocatalytic water splitting by poly(triazine imide) crystals. *Angew. Chem., Int. Ed.* **2023**, *62*, e202304694.

[62] Pan, Z. M.; Zhang, G. G.; Wang, X. C. Polymeric carbon nitride/reduced graphene oxide/Fe_2O_3: All-solid-state z-scheme system for photocatalytic overall water splitting. *Angew. Chem., Int. Ed.* **2019**, *58*, 7102–7106.

[63] Wang, Y. H.; Su, B.; Wang, S. B.; Tan, L.; Zhang, G. G.; Fang, Y. X.; Wang, X. C. Ultralow-content pdcu disordered nanoalloys on carbon nitrides for unity-selective CO_2 hydrogenation to methanol. *Angew. Chem., Int. Ed.* **2025**, *64*, e202508611.

[64] Chi, X.; Lan, Z. A.; Chen, Q.; Zhang, X. R.; Chen, X.; Zhang, G. G.; Wang, X. C. Electronic transmission channels promoting charge separation of conjugated polymers for photocatalytic CO_2 reduction with controllable selectivity. *Angew. Chem., Int. Ed.* **2023**, *62*, e202303785.

[65] Yang, P. J.; Zhuzhang, H. Y.; Wang, R. R.; Lin, W.; Wang, X. C. Carbon vacancies in a melon polymeric matrix promote photocatalytic carbon dioxide conversion. *Angew. Chem., Int. Ed.* **2019**, *58*, 1134–1137.

[66] Yuan, T.; Mei, X. Z.; Liu, K. L.; Fang, Y. X.; Cheng, J. J.; Zheng, M. F.; Wang, X. C. Photofunctionalization of light alkanes by FeO_x/BCN at 12 °C. *J. Am. Chem. Soc.* **2025**, *147*, 35098–35108.

[67] Liu, M. H.; Xu, Y. C.; Liu, Y. X.; Shang, S. C.; Gao, W. Q.; Wang, X. Y.; Hong, J. X.; Xu, H. L.; Hua, C. Y.; You, Z. W. et al. Constructing large-area oriented covalent organic framework based pn heterostructure films to enhance artificial photosynthesis of H_2O_2. *Angew. Chem., Int. Ed.* **2025**, *64*, e202505491.

[68] Hu, X. L.; Zhan, Z.; Zhang, J. Q.; Hussain, I.; Tan, B. E. Immobilized covalent triazine frameworks films as effective photocatalysts for hydrogen evolution reaction. *Nat. Commun.* **2021**, *12*, 6596.

[69] Fang, Y. X.; Li, X. C.; Wang, X. C. Synthesis of polymeric carbon nitride films with adhesive interfaces for solar water splitting devices. *ACS Catal.* **2018**, *8*, 8774–8780.

[70] Fang, Y. X.; Li, X. C.; Wang, X. C. Phosphorylation of polymeric carbon nitride photoanodes with increased surface valence electrons for solar water splitting. *ChemSusChem* **2019**, *12*, 2605–2608.

[71] Fang, Y. X.; Li, X. C.; Wang, Y.; Giordano, C.; Wang, X. C. Gradient sulfur doping along polymeric carbon nitride films as visible light photoanodes for the enhanced water oxidation. *Appl. Catal. B: Environ.* **2020**, *268*, 118398.

[72] Li, X. C.; Wang, J. W.; Xia, J. W.; Fang, Y. X.; Hou, Y. D.; Fu, X. Z.; Shalom, M.; Wang, X. C. One-pot synthesis of CoS_2 merged in polymeric carbon nitride films for photoelectrochemical water splitting. *ChemSusChem* **2022**, *15*, e202200330.

[73] Fan, X. Q.; Wang, Z. L.; Lin, T. E.; Du, D.; Xiao, M.; Chen, P.; Monny, S. A.; Huang, H. M.; Lyu, M. Q.; Lu, M. Y. et al. Coordination chemistry engineered polymeric carbon nitride photoanode with ultralow onset potential for water splitting. *Angew. Chem., Int. Ed.* **2022**, *61*, e202204407.

[74] Battula, V. R.; Mark, G.; Tashakory, A.; Mondal, S.; Volokh, M.; Shalom, M. Binder-free carbon nitride panels for continuous-flow photocatalysis. *ACS Catal.* **2024**, *14*, 11666–11674.

[75] Bojdys, M. J.; Müller, J. O.; Antonietti, M.; Thomas, A. Ionothermal synthesis of crystalline, condensed, graphitic carbon nitride. *Chem.—Eur. J.* **2008**, *14*, 8177–8182.

[76] Li, X. C.; Chen, X. X.; Fang, Y. X.; Lin, W.; Hou, Y. D.; Anpo, M.; Fu, X. Z.; Wang, X. C. High-performance potassium poly(heptazine imide) films for photoelectrochemical water splitting. *Chem. Sci.* **2022**, *13*, 7541–7551.

[77] Su, J. X.; Zhang, J. Q.; Chai, S. M.; Wang, Y. K.; Wang, S. B.; Fang, Y. X. Optimizing poly(heptazine imide) photoanodes using binary molten salt synthesis for water oxidation reaction. *Acta Phys. Chim. Sin.* **2024**, *40*, 2408012.

Data availability

Not applicable.

Acknowledgements

The authors acknowledge the support from the National Key Technologies Research and Development Program of China (No. 2021YFA1502100), the National Natural Science Foundation of China (Nos. 22075047, 22032002, U1905214, and 21961142019), and the 111 Project (No. D16008).

Author contributions

Y. F. L. and Y. N. C. prepared the initial manuscript. G. G. Z. and S. B. W. revised the manuscript. X. C. W. and Y. X. F. supervised the study. All authors have approved the final version of the manuscript.

Competing interests

The authors have no competing interests to declare that are relevant to the content of this article.

Use of AI statement

None.